Journal Pre-proofs

Unravelling the mechanisms of drugs partitioning phenomena in micellar systems via NMR spectroscopy

Katarzyna Malec, Serena Monaco, Ignacio Delso, Justyna Nestorowicz, Marta Kozakiewicz-Latała, Bożena Karolewicz, Yaroslav Z. Khimyak, Jesús Angulo, Karol P. Nartowski

Please cite this article as: K. Malec, S. Monaco, I. Delso, J. Nestorowicz, M. Kozakiewicz-Latała, B. Karolewicz, Y.Z. Khimyak, J. Angulo, K.P. Nartowski, Unravelling the mechanisms of drugs partitioning phenomena in micellar systems via NMR spectroscopy, *Journal of Colloid and Interface Science* (2023), doi: https://doi.org/10.1016/j.jcis.2023.01.063

Unravelling the mechanisms of drugs partitioning phenomena in micellar systems via NMR spectroscopy

Katarzyna Malec[1], Serena Monaco[2], Ignacio Delso[2], Justyna Nestorowicz,[1] Marta Kozakiewicz-Latała[1], Bożena Karolewicz[1], Yaroslav Z. Khimyak*[2], Jesús Angulo*[2,3], Karol P. Nartowski*[1, 2]

[1] Department of Drug Form Technology, Faculty of Pharmacy, Wroclaw Medical University, 211a Borowska Str. 50-556 Wroclaw, Poland

[2] School of Pharmacy, University of East Anglia, Chancellors Drive, NR4 7TJ Norwich, United Kingdom

[3] Instituto de Investigaciones Químicas (CSIC-US), Avda. Américo Vespucio, 49, Sevilla, 41092, Spain

*Correspondence:

Professor Yaroslav Z. Khimyak: School of Pharmacy**,** University of East Anglia**,** Norwich, NR4 7TJ, UK**,**
e-mail: y.khimyak@uea.ac.uk
Professor Jesus Angulo: Institute for Chemical Research (CSIC-University of Seville), 41092 Seville, Spain
e-mail: j.angulo@iiq.csic.es
Dr Karol P. Nartowski: Department of Drug Forms Technology**,** Faculty of Pharmacy, Wroclaw Medical University**,** 211A Borowska Str., 50-556 Wrocław, Poland
e-mail: karol.nartowski@umw.edu.pl

ABSTRACT: Despite extensive use of micelles in materials and colloidal science, their supramolecular organization as well as host-guest interactions within these dynamic assemblies are poorly understood. Small guest molecules in the presence of micelles undergo constant exchange between a micellar aggregate and the surrounding solution, posing a considerable challenge for their molecular level characterisation. In this work we reveal the interaction maps between small guest molecules and surfactants forming micelles via novel applications of NMR techniques supported with state-of-the-art analytical methods used in colloidal science. Model micelles composed of structurally distinct surfactants (block non-ionic polymer Pluronic® F-127, non-ionic surfactant Tween 20 or Tween 80 and ionic surfactant SLS, sodium lauryl sulphate) were selected and loaded with model small molecules of biochemical relevance (i.e. the drugs fluconazole, FLU or indomethacin, IMC) known to have different partition coefficients. Molecular level organization of FLU or IMC within hydrophilic and hydrophobic domains of micellar aggregates was established using the combination of NMR methods (1D 1H NMR, 1D 19F NMR, 2D 1H-1H NOESY and 2D 1H-19F HOESY, and the multifrequency-STD NMR) and corroborated with molecular dynamics (MD) simulations. This is the first application of multifrequency-STD NMR to colloidal systems, enabling us to elucidate intricately detailed patterns of drug/micelle interactions in a single NMR experiment within minutes. Importantly, our results indicate that flexible surfactants, such as block copolymers and polysorbates, form micellar aggregates with a surface composed of both hydrophilic and hydrophobic domains and do not follow the classical core-shell model of the micelle. We propose that the magnitude of the changes in 1H chemical shifts corroborated with interaction maps obtained from DEEP-STD NMR and 2D NMR experiments can be used as an indicator of the strength of the guest-surfactant interactions. This NMR toolbox can be adopted for the analysis of the broad range of colloidal host-guest systems from soft materials to biological systems.

INTRODUCTION

Micelles have many advantages as nanosize (below 200 nm) drug delivery systems, *e.g.* solubility enhancement of sparingly soluble active pharmaceutical ingredients (APIs), modified drug release or targeted delivery of molecules to their site of action.[1–3] Drug solubilization within micelles is a spontaneous process of incorporating the drug into micelles resulting in the thermodynamically stable system. The localization of a drug within the micelle depends primarily on the drug polarity.[4] The local differences within the micelle structure promote the

formation of sites with different polarities enabling drug partitioning. Therefore, interactions between surfactant and drug do not appear at determined binding site.[4] Moreover, there is dynamic equilibrium of drug molecules being in a constant exchange between the aqueous and micellar phase.[5] Therefore, understanding transient structure of micelles and their interactions with drug molecules at atomistic level requires application of complementary analytical techniques enabling to probe that supramolecular organisation.

Nuclear Magnetic Resonance (NMR) spectroscopy is a sensitive tool for probing molecular recognition and to obtain information on structure, dynamics and local environment of interacting species e.g. drug-protein[6,7] and protein-protein[8], multicomponent supramolecular gels[9,10] or host-guest systems.[11,12] The magnitude of chemical shift perturbations can be used to determine the affinity and binding site of the ligand to protein.[13] This approach has been transferred to micellar systems in which slight changes in local electronic environment triggered by the interactions between drug and surfactant molecules can be detected in high-resolution NMR as changes in chemical shifts, appearance of new signals or broadening of the peaks in 1D proton spectra.[14] Furthermore, transferred NOE spectra have been reported as a tool for determination of drug localization within micelles based on the analysis of intramolecular drug-surfactant cross-peaks present in 2D NMR spectra that indicate spatial proximity of interacting species.[15] Changes in diffusion coefficients assessed with PFG NMR (Pulsed-field gradient NMR) can also help to confirm drug incorporation into the micelles or to determine partitioning of drug between micelles and solution.[5,16] In addition, measurements of relaxation time (T_1) enable observation of changes in dynamics of block polymer chains upon micellization process[17] Saturation Transfer Difference NMR (STD NMR) is an emerging technique for determination of transient interactions in colloidal systems. To date this approach has been used for liposaccharide micelles (LPS) comprising endotoxin in bacterial membrane to map the binding surface of antimicrobial peptides (AMP).[18–23] STD NMR is used frequently for monitoring weak ligand binding (dissociation constant, K_D, ranging from 10^{-8} mol L^{-1} to 10^{-3} mol L^{-1}) to protein receptor and is used extensively in screening for biologically active molecules and new drug candidates enabling to establish their protein binding affinity.[24,25] This method relies on saturation transfer from protein or peptide receptors (>20 kDa) to low molecular weight ligands via nuclear Overhauser effect. In addition, epitope mapping that might be obtained after data processing indicates the strength of interactions of ligand's particular parts at the binding site of protein.[26] Recently developed DEEP-STD NMR (DiffErential EPitope mapping by STD NMR spectroscopy) enables identification of the residues contacting the bound ligands, as opposed to traditional STD NMR that only depicts the binding epitope mapping of the ligand. If the binding site architecture is known, the ligand orientation in the binding pocket can be defined.[27] In this work we demonstrated novel use of DEEP-STD NMR to soft colloidal nanomaterials which resemble the structure of macromolecules i.e. micelles. In contrary to protein-ligand interactions, in micellar formulations, the receptor is formed *in situ* and remains in fast exchange with monomers in the solution. Furthermore, several transient binding sites for drug molecules can be present within the micelles structure in contrast to a well-defined binding pocket that is normally observed in protein structures. In addition to NMR, computational Molecular Dynamics can illustrate and explain the behaviour of colloidal systems observed experimentally. Most of MD studies described so far in literature follow the coarse-grained MD approach, due to the size and complexity of the systems.[28,29,30,31,32] However, this protocol is known to show a low accuracy in the atomistic level, not suitable for the kind of intermolecular interactions observed by NMR. The use of traditional atomistic level MD increases the computational cost of the simulations enormously.[33,34] However, it also provides a better description of the structure and dynamic processes.[35]

The aim of this study was to develop new tools to investigate transient interactions within soft colloidal materials that can be used across different delivery systems from micelles to vesicles and nanoemulsions. Four different surface-active agents classified as different types of surfactants varying in the structure, molecular weight, critical micellar concentration and solubilization efficacy were chosen as model micelle forming agents. A wide range of surfactant concentrations was investigated to understand the solubilization process of model drugs at different stages of the micellization process (from values close to CMC to values 20-2500 times larger than CMC depending on the surfactant). The magnitude of the changes in ^{1}H chemical shifts are proposed as the indicator of the strength of the interaction between a drug and a surfactant in a micelle, following the same concept widely used to probe protein-ligand interactions. These data agree with micellization driven drug solubility increase (as

2

determined by HPLC). Our innovative application of DEEP-STD NMR to micellar systems, enabled us to determine an intricately detailed pattern of drug/micelle interactions in a single NMR experiment within minutes. The experimental data were consistent with the atomistic level Molecular Dynamics study providing a model that might illustrate and explain the behaviour of the investigated systems. The proposed approach can be translated to other colloidal systems that span from pharmaceuticals and microorganisms to consumer products and foods.
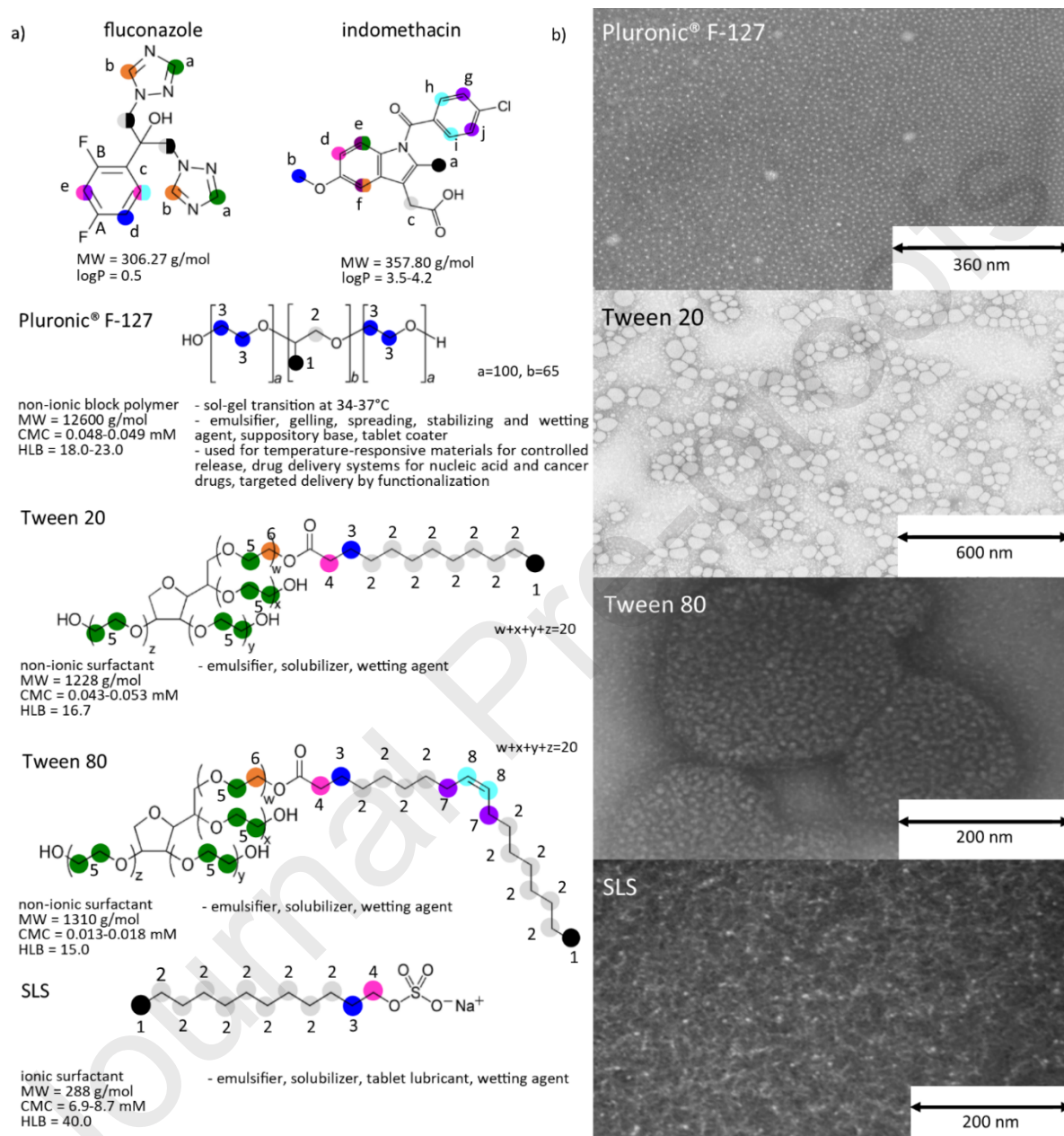

Figure 1. (a) Structure of drugs and surfactants comprising investigated micellar systems with their applications in drug delivery.[36,37,38,39] (b) TEM images of surfactants at concentrations above CMC: Pluronic® F-127 at 0.063 mM, Tween 20 at 0.12 mM, Tween 80 at 0.060 mM and SLS at 12 mM.

RESULTS AND DISCUSSION

CMC of the selected model systems determined using surface tension measurements and fluorescence spectroscopy were in agreement with previously published data (ESI, Figure S1 and Table S1). It is worth noting that the heterogeneity of the polymers and polysorbates (namely the presence of molecules differing with the polarity, e.g. diblocks in the first case and a mixture of oligomers in the latter case)[40–44] might affect micellization process and the CMC values. That is the reason why CMC established for the investigated surfactants covers a

broad range of values in the literature (ESI, Table S1). We observed formation of spherical micelles in all our systems as shown in TEM images (Figure 1 and ESI, Figure S2-S7). At concentrations below the determined CMC no micelles were detected in TEM images. The size of the micelles determined by DLS was consistent with the size of the micelles measured in TEM images (see ESI, section 'DLS measurements and TEM images' for details).

The atomistic model of micelles was obtained from multidimensional NMR spectroscopy supported with MD simulations (see ESI, section 'NMR results, MD simulations and HPLC results', Table S3-S6, Figure S8-S17). The changes in chemical shifts ($\Delta\delta$) of ^{1}H sites in the surfactant measured as a function of increasing surfactant concentration implied considerable changes in the local environment of interacting species upon formation of micellar aggregates (ESI, Figure S8-S9). We have built micellar models based on Pluronic® F-127, Tween 20, and SLS (Figure 2 and ESI, section 'Methods'). Tween 80 was not included in the simulated systems due to its similarities with Tween 20. Our data suggest that complex and flexible molecules such as block copolymers and polysorbates did not follow the classical core-shell model of the micelle, where surfactants segregate to form supramolecular assemblies with distinct properties, but rather dynamic domains of distinct hydrophobicity were formed at the micelle surface being exposed towards water as shown in Tweens and Pluronic systems. These data not only provided a basis for understanding drug-micelles interactions as described in this work but have general and far-reaching implications in understanding of other host-guest systems that use flexible molecules of distinct polarities as building blocks proving the critical role of the surface interactions in soft colloidal nanomaterials dispersed in aqueous media.
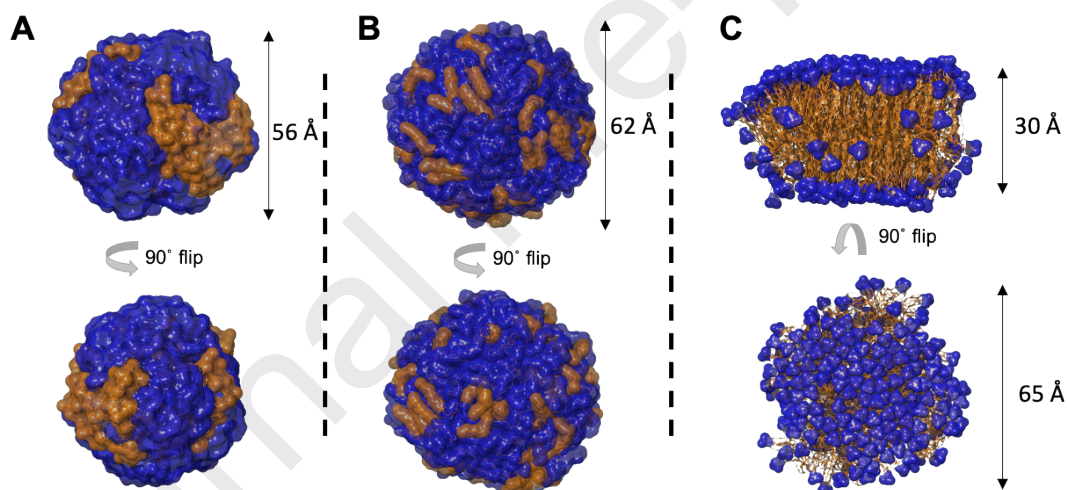
Figure 2. Representation in two different views of micelles after 50 ns of MD simulation, with the average measures of the micelles along the last 10 ns of the simulation. Explicit water molecules have been removed for clarity. a) Pluronic® F-127: PEO polar chains are represented as blue surfaces and PPO chains are shown as orange surfaces. b) Tween 20: PEO chains are represented as blue surfaces and lauryl hydrophobic groups are shown as orange surfaces. c) SLS: Hydrogen atoms have been removed for clarity. Lauryl chains are represented as orange surfaces and sulphate groups as blue surfaces.

Probing drug-surfactant interactions in micellar systems.

The effect of FLU loading into micelles on the chemical environment of both components was investigated in the series of ^{1}H NMR experiments with 6.5 mM, 13 mM and saturated solution of FLU at selected surfactant concentrations. Only one series of the saturated solution of IMC was studied since its saturation solubility was strongly dependent on surfactant concentration due to IMC's overall very low solubility in water. Assignment of the ^{1}H peaks is presented in ESI, Table S7-S10 and Figure S18-S19. ^{1}H-^{1}H NOESY and ^{1}H-^{19}F HOESY experiments were acquired for selected formulations resulting in the generation of the spatial map of drug-surfactant interactions. Small molecules are characterized by rapid tumbling (ESI, Figure S20-S21) and display positive NOE

4

(possessing the opposite sign to the diagonal) whereas slowly tumbling large molecules show negative NOE (characterized by the same phase as the diagonal). Therefore, negative NOE observed for the drug in the presence of surfactants may indicate incorporation of drug molecules into micelles.

Pluronic®F-127 micelles loaded with FLU or IMC.

In micelles composed of Pluronic® F-127 at concentrations up to 4.0 mM loaded with FLU or IMC, the most pronounced changes were observed for methyl and methylene polymer protons of propoxy blocks (signals 1 and 2). In contrast, protons of ethoxy groups (signal 3) experienced only minor changes in local environment regardless of the level of drug loading (Figure 3a, 4a, and ESI, Table S7). 2D NOESY spectrum of 19 mM FLU in 4.0 mM Pluronic® F-127 exhibited the cross-peaks same-phased as diagonal between FLU protons and those of propoxy block of the polymer (ESI, Figure S22b) indicating spatial vicinity of the drug and surfactant molecules. In contrast, no intermolecular cross-peaks were observed in 2D NOESY spectra at lower Pluronic® F-127 concentrations (0.095 mM and 0.79 mM with 18.1 and 18.3 mM of FLU respectively, ESI, Figure S22a), and cross-peaks between surfactant protons were opposite phased to diagonal, similarly to assemblies of polymer without the drug, indicating that polymer aggregates formed below 0.79 mM did not resemble the macromolecular assembly. Interactions between Pluronic® F-127 at 4.0 mM and IMC (0.54 mM) were proven via cross-relaxation between most drug protons (except H_c) and those in PPO and PEO blocks of polymer (ESI, Figure S23). NOE cross-peaks of the same phase as the diagonal indicated intermolecular interactions. Comparably to FLU series, no intermolecular cross-peaks were observed in the 2D NOESY spectrum of 0.023 mM IMC loaded into 0.095 mM polymer (i.e. slightly above CMC) and intramolecular cross-peaks between polymer were opposite phase to the diagonal.

Tween 20 and Tween 80 micelles loaded with FLU or IMC.

Shielding of Tween 20 signals 3, 4 and 6 ($\Delta\delta$ = 0.020; 0.034 and 0.022 ppm respectively) was observed when 13 mM of FLU was added to 0.060 mM surfactant solution (ESI, Figure S24a). Similar deshielding of signal 3 (-0.09 < $\Delta\delta$ < -0.06 ppm) and shielding of signal 4 (0.023 < $\Delta\delta$ < 0.031 ppm) occurred upon interactions between FLU (13 mM) and Tween 80 near CMC (0.015-0.025 mM) (Figure 3d). At 8.1-41 mM (Tween 20) and 7.6-38 mM (Tween 80) surfactants concentration addition of 13 mM FLU resulted in smaller changes in the position of Tweens protons (-0.005 < $\Delta\delta$ < 0.02 ppm at 41 mM and 38 mM, respectively for Tween 20 and Tween 80) (ESI, Table S8-S9), suggesting that the addition of drug at surfactant concentrations near CMC induces structural rearrangements of colloidal particles, commonly known as hydrophobic effect.[45] At surfactant concentrations around CMC (0.080-0.24 mM and 0.006-0.025 mM for Tween 20 and Tween 80, respectively) only intramolecular (drug–drug or surfactant-surfactant) cross-peaks were observed in the NOESY spectra and maintained their positive and negative phases, respectively (ESI, Figure S25-S27). Above CMC in both systems loaded with FLU, cross-peaks of the same phase as diagonal were observed in the NOESY spectrum between all drug protons and methylene protons in ethoxy group and aliphatic chain of surfactant (signals 2, 5). These intermolecular contacts were observed across the broad range of evaluated concentrations of Tween 20 (8.1-41 mM) and Tween 80 (23 and 38 mM), see ESI, Figure S25-S27. Upon increasing concentration of Tweens the ratio between inter- and intramolecular contacts increases (e.g. FLU protons and protons 1, 3, 4, 6 in both Tweens and additionally signals 7, 8 in Tween 80). Those findings confirmed the enhanced affinity of FLU to surfactant molecules upon increased surfactant concentration explained by drug solubility improvement (as indicated in Figure 5 and ESI, Figure S28).

The pattern of changes observed for IMC loaded micelles was similar to those detected in FLU-Tweens systems. Shielding of signals 3 (0.036 < $\Delta\delta$ < 0.052 ppm) and 4 (0.011 < $\Delta\delta$ < 0.030 ppm) attached to carbonyl group appeared upon loading IMC into Tween 20 micelles at concentrations near CMC (0.80-0.120 mM). Addition of IMC to Tween 80 around CMC at 0.020-0.025 mM led to deshielding of signal 3 (-0.019 < $\Delta\delta$ < -0.039 ppm). Major rearrangements concerned signal 6 (0.052 < $\Delta\delta$ < 0.059 ppm) followed by shielding of signals in aliphatic chain (7: 0.021 < $\Delta\delta$ < 0.033 ppm, 8: 0.028 < $\Delta\delta$ < 0.030 ppm, 1 and 2 in the range 0.017 < $\Delta\delta$ < 0.024 ppm). In both Tweens (at 41 mM and 38 mM, respectively) signals 3, 4 and 6 in proximity to carbonyl group experienced perturbation upon interactions with IMC (upfield shift of $\Delta\delta$ = 0.033-0.048; and $\Delta\delta$ = 0.037-0.048 for Tween 20 and 80 respectively) followed by changes in aliphatic chain (Figure 4d and ESI, Figure S29a and Table S8-S9).

5
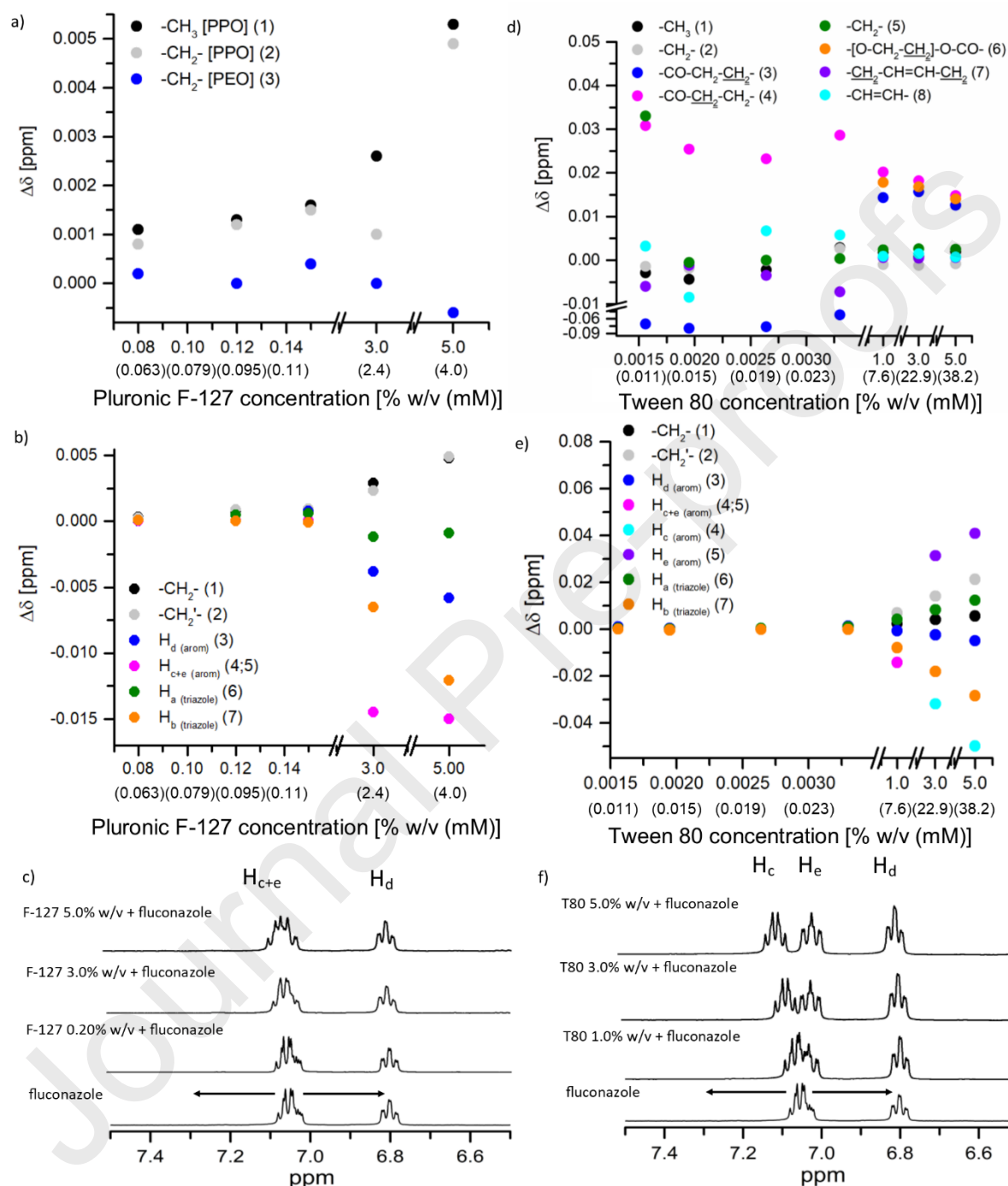
Figure 3. Change in ^{1}H chemical shifts in surfactants and FLU in surfactant solutions loaded with 13 mM FLU: (a, b) Pluronic® F-127 (up to 5.0% w/v, 4.0 mM), (d,e) Tween 80 (up to 5.0% w/v, 38 mM). ^{1}H NMR spectra of (c) Pluronic® F-127 solution and (f) Tween 80 solution loaded with 13 mM FLU.
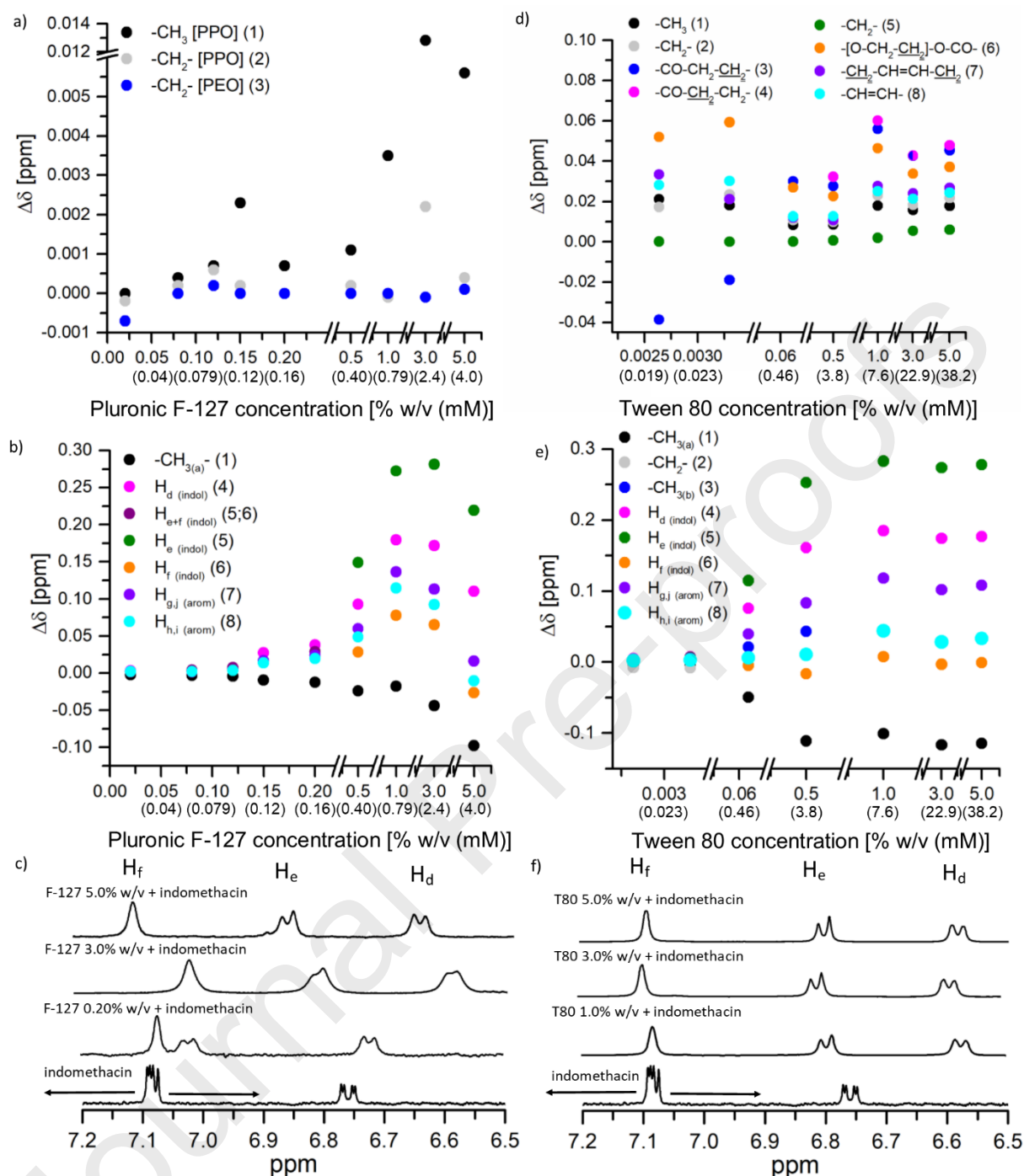
Figure 4. Change in ^{1}H chemical shift in surfactants and IMC in surfactant solutions: (a, b) Pluronic® F-127 (up to 5.0% w/v, 4.0 mM) loaded with 0.012-0.54 mM IMC, (d, e) Tween 80 (up to 5.0% w/v, 38 mM) loaded with 0.045-3.1 mM IMC. ^{1}H NMR spectra of (c) Pluronic® F-127 solution loaded with 0.031-0.54 mM IMC and (f) Tween 80 solution loaded with 0.66-1.1 mM IMC.

Remarkably, at surfactant concentrations around CMC for Tween 20 and 0.006-0.025 mM Tween 80 with FLU and IMC (ESI, Figure S25a, S27a, S30a, S31a) no intermolecular drug-surfactant cross-peaks were present. In Tween 20 and 80 solution (41 mM and 38 mM) IMC (from 0.027 to 3.1 mM) and Tween 80 with FLU (23 mM), drug-surfactant and drug-drug cross-peaks shared the same phase as diagonal presumably because of viscosity increase affecting the tumbling rate of all components within the system including drug molecules in bulk solution (ESI, Figure S27b and Figure S30b-S31b). For IMC loaded micelles in the NOESY spectrum drug-drug and drug-surfactant cross-peaks were observed between all drug protons and all surfactant protons in both Tween 20 and Tween 80 indicating multiple interactions in the dynamic micellar assembly. The effect of spin diffusion

and chemical exchange on the appearance of cross-peaks was excluded in ROESY experiments (ESI, Figure S32-S34).

SLS micelles loaded with FLU or IMC.

The addition of FLU into SLS micelles resulted in shifts of SLS peaks assigned to hydrophilic head of a surfactant ($\Delta\delta$ = 0.065 and 0.044 ppm for signal 3 and 4 respectively, ESI, Figure S24e and Table S10). In 2D NOESY spectra FLU-SLS cross-peaks between aromatic protons with signal 2 of SLS were observed (15 mM surfactant with 21 mM FLU). Besides, drug-drug cross-peaks opposite phased to a diagonal were observed (between -CH_2-/-CH_2'- and both aromatic rings, see ESI, Figure S35a). At higher SLS concentrations 104 mM and 173 mM addition of 43 mM and 60 mM FLU, respectively, resulted in additional weak NOE signals between drug and SLS protons (signals 1, 3 and 4) while contacts between -CH_2-/-CH_2'- and triazole ring within drug remained (ESI, Figure S35b). The NOESY cross-peaks of both phases were observed regardless of the surfactant and drug concentration, similarly to SLS samples without the drug at the concentration well above CMC.

The addition of IMC into SLS micelles resulted mostly in an upfield shift of the hydrophobic parts of the SLS molecules (at 15 mM, near CMC, $\Delta\delta$ = 0.014 and 0.018 ppm for signals 1 and 2 respectively, ESI, Figure S29d and Table S10). 2D NOESY spectrum of 173 mM SLS with 5.0 mM IMC (ESI, Figure S33b) micellar solution displayed cross-peaks between methylene protons in SLS (signal 2 in Figure 1a) and all IMC protons confirming their spatial proximity in micelles. This differed from the 15 mM surfactant and 0.41 mM IMC solutions, where only drug-drug interactions were observed (ESI, Figure S36a). The increase of SLS concentration resulted in changes of drug-drug cross-relaxation map. At 15 mM SLS cross-peaks between H_c with H_f/H_a were detected whereas at 173 mM additional cross-peaks between H_a, H_f and chlorobenzene ring; H_c with $H_{h,l}$ and H_b with indole ring were observed.

Changes in the local environment of FLU and IMC upon partitioning in surfactant systems.

Substantial changes in local environment of several FLU protons within all micellar system were observed. These include shielding of H_e and deshielding of both H_c and H_b protons (Figure 3 and ESI, Figure S24 and Table S7-S10). For micelles containing IMC, a substantial upfield shift of H_d and H_e protons in indole ring of IMC was observed (Figure 4 and ESI, Figure S29). In the presence of 173 mM SLS H_e experienced major perturbation (around 0.05 ppm). Based on 1D NMR data, hydrophobic motifs of both FLU and IMC interacted with micelles as demonstrated by the substantial changes in their ^{1}H chemical shifts of protons. For example, overlapping signals H_c and H_e in fluorobenzene ring of FLU might be distinguished upon an increased concentration of the surfactants (Figure 3 and ESI, Figure S24). Overlapped indole signals H_e and H_f in IMC (Figure 4 and ESI Figure S29) were also separated in ^{1}H NMR spectra recorded at higher surfactant concentrations. Broadening of IMC signals was also observed (e.g. in Figure 4c, 4f, and ESI Figure S29) presumably due to drug-micelles interaction (discussed further). We observed that the higher the drug solubilization in the micellar system, the larger change in chemical shift value ($\Delta\delta$) (Figure 3-4 and ESI, Figure S24, S29, S37-S38). This suggests that $\Delta\delta$ can be used as a measure of drug partitioning into the micelles.

Changes observed in ^{1}H NMR were corroborated by ^{19}F NMR spectra of FLU. In both Tween systems at highest investigated concentrations, upfield shift of F_A ($\Delta\delta$ = 0.13-0.16) and downfield shift of F_B ($\Delta\delta$ =0.13-0.14) were seen upon addition of 13 mM FLU (ESI, Figure S39 and Figure S24d). Those results agree with spectral changes observed for H_e and H_c protons that were close to F_A and F_B, respectively. In SLS system at 173 mM loaded with 23 mM FLU signals from fluorine were shifted downfield (F_A, $\Delta\delta$ = 0.44 and F_B, 0.027 ppm) (ESI, Figure S24h).
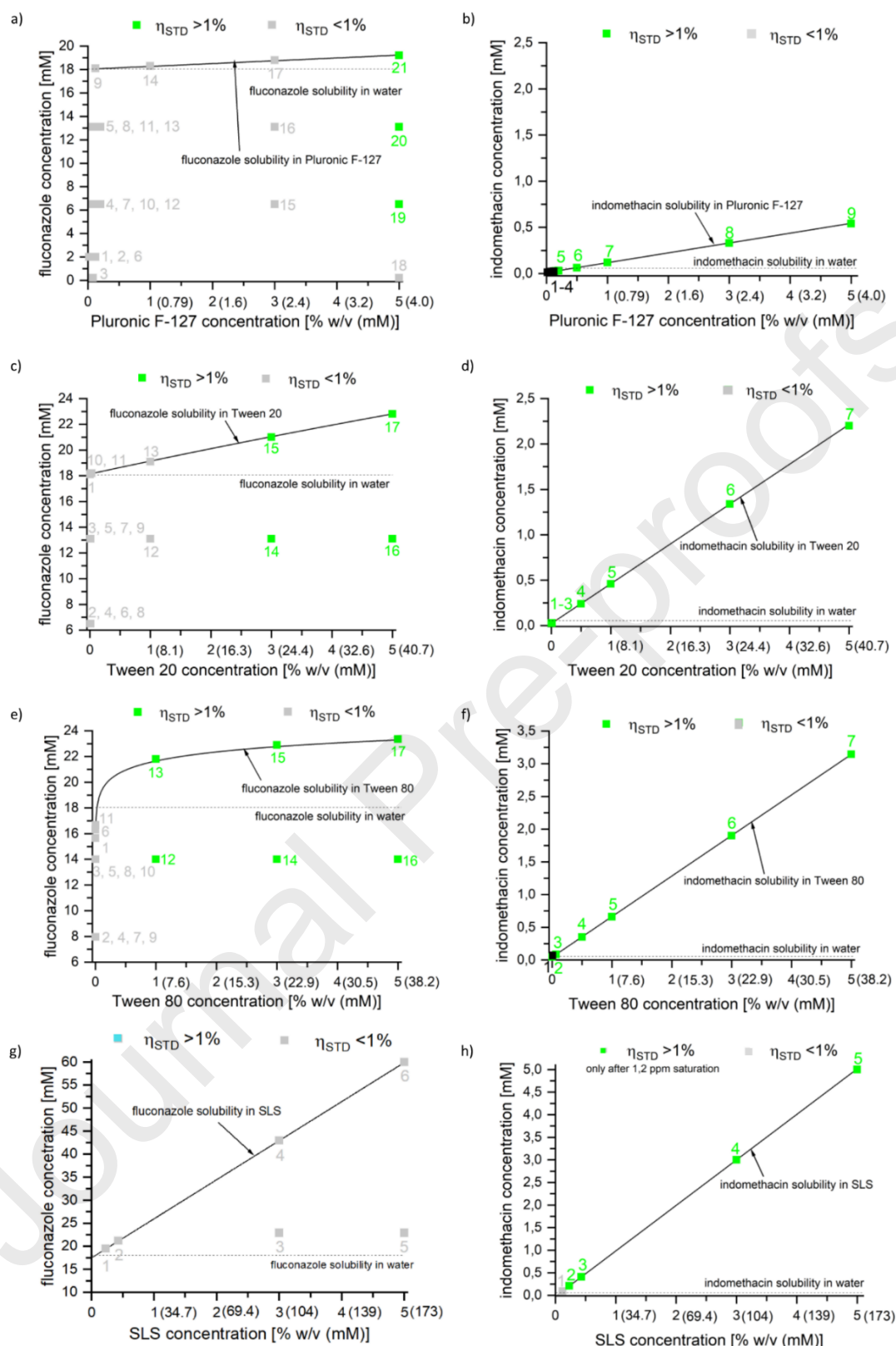
Figure 5. FLU solubility within (a) Pluronic® F-127, (c) Tween 20, (e) Tween 80 and (g) SLS solutions measured by HPLC. IMC solubility within (b) Pluronic® F-127, (d) Tween 20, (f) Tween 80 and (h) SLS solutions established by HPLC. Data are correlated with STD NMR measurements. Samples with vague peaks of drugs in difference spectra are marked with black squares. The numbers on the graphs correspond to the numbers of the examined samples summarized in ESI, Table S11-S18.

Overall, 1D NMR data together with ^{1}H-^{1}H NOESY NMR spectra indicated which structural motifs in the drug and surfactant were primarily involved in drug-surfactant interactions. The latter confirmed FLU and IMC incorporation into micelles, especially at surfactant concentration well above the CMC values. In IMC series (at concentration above CMC), both drug-surfactant as well as drug-drug cross-peaks shared the same phase as diagonal. This can be explained by higher logP value of IMC as compared to FLU, resulting in different solubilities of both drugs in surfactant solutions (see Figure 5 and ESI, Figure S40). This indicates increased drug incorporation into the micelles. The intensities of FLU -CH$_2$-/-CH$_2$'- and H$_{c+e}$, H$_a$, H$_b$ drug-drug cross-peaks varied among investigated samples depending on surfactant concentration while retaining the same map of drug-drug contacts. ^{1}H-^{1}H NOESY findings were in agreement with ^{1}H-^{19}F HOESY spectra acquired for selected formulations. The data confirmed the interactions between fluorine F$_A$ and F$_B$ of FLU and Tween 20 (cross-peak arisen from cross-relaxation of F$_A$ and F$_B$ and methylene protons in ethoxy group) within micellar system composed of 41 mM surfactant and 23 mM FLU, whereas no intermolecular cross-peaks were observed in 18 mM FLU loaded into 0.095 mM Pluronic® F-127 in agreement with ^{1}H-^{1}H NOESY data. The 2D ROESY spectra confirmed that all observed cross-peaks resulted from through-space interactions and not from spin diffusion or chemical exchange processes (ESI, Figure S32-34).

DEEP-STD NMR investigation of drug micelles systems.

We have used DEEP-STD NMR to investigate the interactions between drug and surfactant within micellar systems assuming that saturation transfer within those supramolecular assemblies might be as effective as in proteins (Figure 6a).[46] To translate DEEP-STD NMR experiments to drug-micelle systems, the surfactant species in the micelles were regarded as supramolecular receptor while the interacting drug as the ligand. The chosen irradiation frequencies were characteristic for the hydrophilic and hydrophobic parts of their structure. This enabled us to evaluate in which region of the micelle the drug resides preferentially.

Following the DEEP-STD NMR protocol, two STD NMR experiments were run at two different frequencies for each formulation, and the DEEP-STD factors (ΔSTD) were calculated for each proton site in the drug. Mapping DEEP-STD factor onto the structure of the drug yielded the differential epitope map of a drug. One must bear in mind that only drug protons resonating far from the irradiated surfactant signal (Δδ at least 1 ppm) must be included in the ΔSTDs calculations to avoid false positive signals arising from direct irradiation.[47] Only drug protons not affected by the spread of direct saturation in control measurements were taken into consideration in this work.

For FLU, the ΔSTDs suggest affinity of the triazole proton H$_a$ for the hydrophobic region of both Pluronic® F-127 (propoxy blocks) and Tweens (aliphatic chains) (Figure 6c and ESI, Figure S41-S43). In contrast, triazole proton H$_b$ and aromatic proton H$_c$ were directed towards hydrophilic parts of surfactants' structure such as ethoxy groups in Pluronic® F-127 and ethoxy monomers attached to sorbitan ring in the investigated Tweens. For the systems in which the signals of H$_e$ and H$_c$ were overlapped, ΔSTD could not be evaluated separately (ESI, Figure S41 and S43). In both Tween systems, aromatic protons H$_e$ and H$_d$ point towards the hydrophobic part of the surfactants, in contrast to Pluronic® F-127 micelles where the H$_d$ ΔSTD was close to 0 (ESI, Figure S41). In micellar systems loaded with FLU protons -CH$_2$- of the drug were excluded from the analysis because of their proximity in spectra to the peaks of surfactants that were irradiated.

DEEP-STD NMR analysis of Pluronic® F-127 and Tween micellar solutions with IMC indicated H$_d$ and H$_e$ protons in indole ring was directed towards the ethoxy blocks and the hydrophilic ethoxy monomers attached to sorbitan ring. In contrast H$_g$, H$_h$, H$_i$ and H$_j$ in phenyl ring seem to point towards hydrophobic propoxy blocks and aliphatic chain in Pluronic® F-127 and Tween (Figure 6c and ESI, Figure S44-S46). IMC protons H$_a$, H$_b$ and H$_c$ in formulations were excluded from the analysis, due to their proximity to the peaks of surfactants that were irradiated. To avoid such direct irradiation being transferred to H$_f$ through space it has also been excluded from the analysis. In NMR spectra of all three surfactants at concentrations near CMC H$_e$ and H$_f$ protons overlapped. Therefore, in these formulations ΔSTD for both protons could not be calculated separately (ESI, Figure S45-S46).
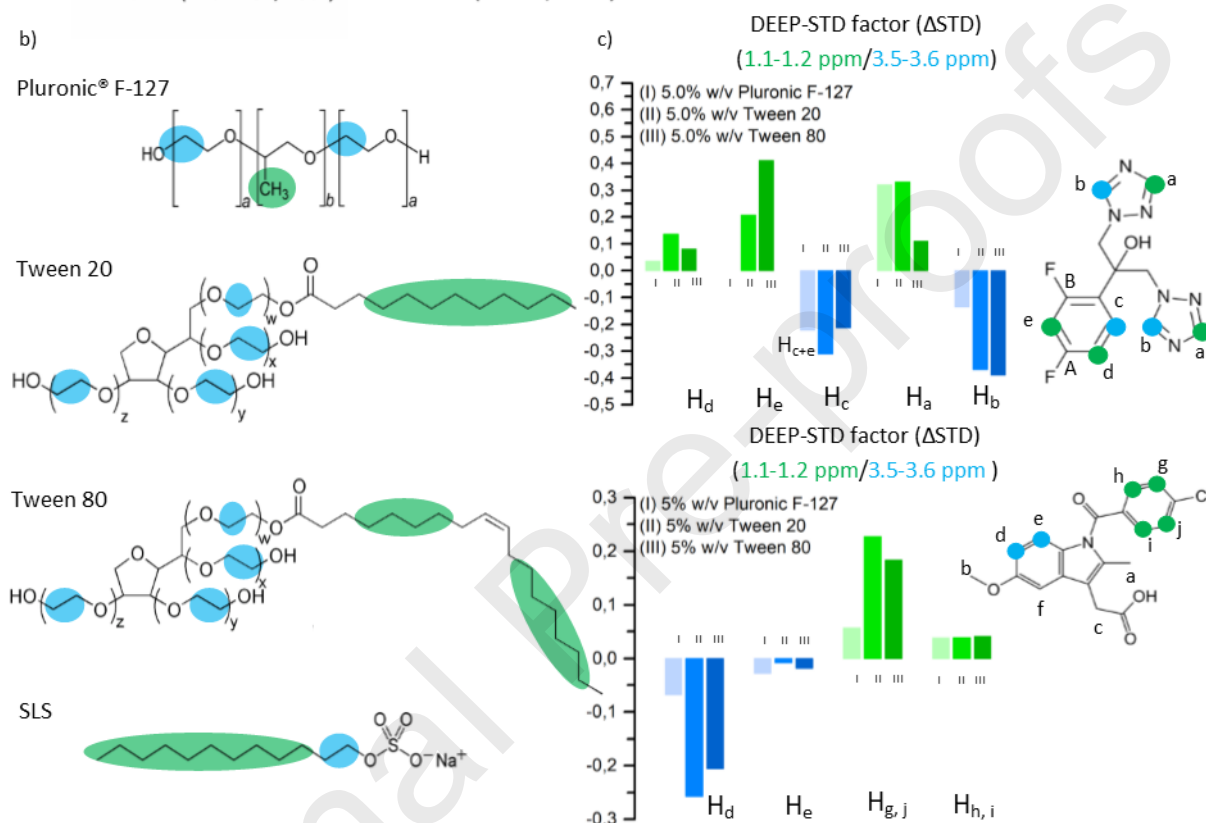
Figure 6. (a) Scheme of STD experiments investigating ligand-protein/micelle-drug interactions. (b) Structure of Pluronic® F-127, Tween 20, Tween 80, SLS with hydrophilic parts in green frame and hydrophobic parts in blue frames irradiated during experiments. (c) DEEP-STD factor of FLU and IMC within micellar systems composed of 4.0 mM Pluronic® F-127, 41 mM Tween 20, and 38 mM Tween 80.

While each model drug displayed a distinct pattern of the contacts upon irradiation of the hydrophilic or hydrophobic part of the micelle, the map of contacts obtained in DEEP-STD NMR experiments was similar among the studied surfactants (Figure 6). This suggests similar orientation of the drug towards hydrophilic and hydrophobic parts of the micelles. The obtained map of interactions was consistent across the investigated surfactant concentrations regardless of the surfactant used (Figure S41-S46).

Calculated DEEP-STD factors correlated well with the data of ^{1}H NMR chemical shifts perturbation. Analysis of the ΔSTDs of FLU revealed that throughout the studied formulations, protons H_b and H_c exhibited proximity to the hydrophilic part of surfactants whereas protons H_a and H_e were involved in interactions with hydrophobic moieties in surfactant. Based on ^{1}H chemical shift changes, protons H_b and H_c experienced deshielding (Figure 3-4 and ESI, Figure S24 and S38) most likely from neighboring electronegative oxygen in hydrophilic ethoxy groups. Accordingly, H_a and H_e were shifted upfield in 1D ^{1}H NMR spectra. Furthermore, protons in IMC series

for which ΔSTD was calculated exhibited the largest perturbation in local environment meaning the largest changes in chemical shifts in ^{1}H NMR spectra (Figure 4 and ESI, Figure S29). Although FLU and IMC were localized between hydrophilic and hydrophobic parts of surfactants' structures, the majority of protons in more hydrophobic IMC was found to interact with hydrophobic moieties of the surfactants. Previous models of micelles postulated that polar molecules are solubilized preferentially in palisade layer,[48] while our NMR and MD (see below) data suggested that drug molecules can undergo partitioning between hydrophilic and hydrophobic domains at the micelles surface.

Molecular Dynamic simulations of micelles loaded with fluconazole or indomethacin.

Micelle models loaded with FLU or IMC showed the same behaviour as pure micelles (ESI, Section 5). In few cases, due to the way of forming the micelles, some drug molecules were trapped inside the micelles and were not able to diffuse to the surface. However, this did not affect to the overall micelle dynamics and shape, except in the case of Tween 20 in presence of IMC (discussed below).

At 30 ns of simulation, all the studied systems yielded a stable structure, and only the drug molecules showed some fluctuation on the surface of the micelles. Therefore only the last 20 ns of each simulation will be considered for the description of each micellar system.
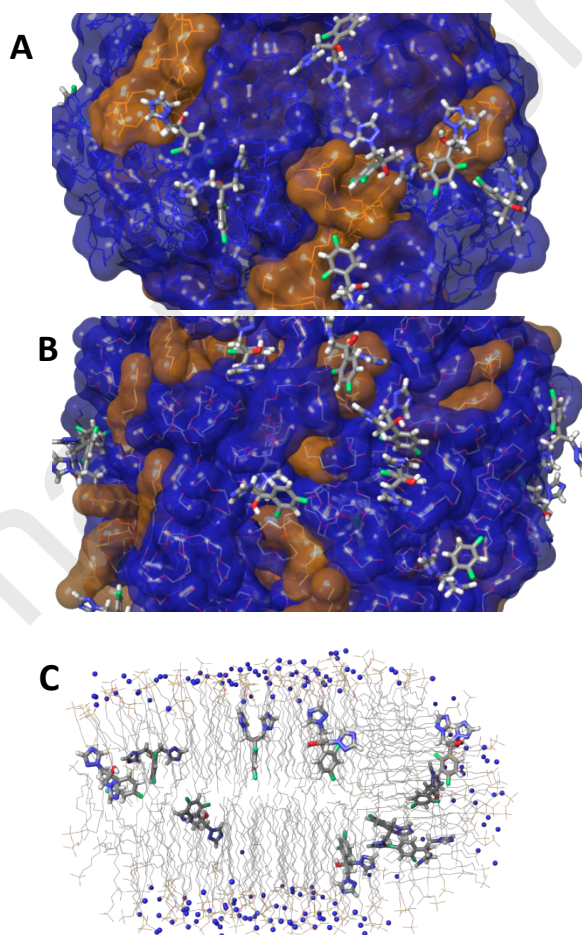
Figure 7. Snapshots at 50 ns of the MD simulation with the micelles loaded with FLU, corresponding to Pluronic® F-127 (a), Tween 20 (b) and SLS (c). FLU is represented in thick tubes, and explicit water molecules have been removed for clarity. PEO polar chains are represented as blue surfaces and hydrophobic PPO and lauryl chains are shown as orange surfaces for Pluronic® F-127 and Tween 20. Sodium ions are shown as blue spheres in the SLS system.

FLU molecules showed a random distribution across the Pluronic® F-127 micelle surface, with no distinct preference towards the hydrophobic or hydrophilic domains (Figure 7a). However, those FLU molecules close to propoxy chains showed a preferred conformation pointing the difluorophenyl ring towards the micelle core, in closer contact with the hydrophobic blocks (ESI, Figure S47). Similarly, FLU molecules in presence of the Tween 20 micelle did not show a structured pattern, probably due to the homogeneous distribution of hydrophobic and hydrophilic chains on the micelle surface (Figure 7b and ESI, Figure S48).

When incorporated into SLS micelles, FLU molecules were located preferentially at disordered edges of the micelles, as lauryl chains were partially exposed to the solvent (Figure 7c). Also, in most of FLU molecules, difluorophenyl moiety was oriented parallel to the hydrophobic chains, while triazole rings were exposed to the surface. This arrangement was in agreement with the higher chemical shift displacement observed for the methylene groups closer to sulphate in SLS (ESI, Figure S49).

The block co-polymeric nature of Pluronic® F-127 and Tween 20 resulted in the formation of compact micellar aggregates that were not permeable for drug or water molecules. Hence, addition of drugs to the preformed micelles led to a surface interaction in all cases, except in the case of SLS aggregates.

To study the effect of pH on the interaction between IMC and the micelle, both protonation states of IMC were simulated. As both cases displayed the similar behaviour, only the results for the ionised IMC were described, as it is the main protonation state at neutral pH.

During the formation of Pluronic® F-127 micelles few molecules of IMC were trapped inside the micelle, but this did not affect the properties and dynamics of the overall micelle. During the last 20 ns of the simulation, all IMC molecules were distributed over the micelle surface without showing any preference for hydrophilic or hydrophobic blocks (ESI, Figure S50). The most populated conformation for Pluronic® F-127 placed the indole ring parallel to the micelle surface, with the 4-chlorobenzamide ring out of the indole plane and partially buried in small clefts on the micelle surface (Figure 8a).

The Tween 20 micelle formed in presence of IMC showed a more homogeneous distribution of the laureate chains over the micelle surface, reducing the size of hydrophobic aggregates. Hence, the probability of finding IMC molecules close to laureate groups or PEG chains was very similar, as all the drug molecules were distributed homogeneously around the micelle (Figure 8b and ESI, Figure S51).

When interacting with SLS, most of IMC molecules were placed on the edge surroundings, similarly to FLU, where they can get close the hydrophobic chains without going through the high-polar sulphate layer, and avoid the proximity of the SLS sulphate groups to the IMC carboxylate, both negatively charged (ESI, Figure S52). The charged carboxylate was exposed to solvent, while both the 4-chlorophenyl ring and the methoxy group point towards the micelle centre, surrounded by hydrophobic chains (Figure 8c).
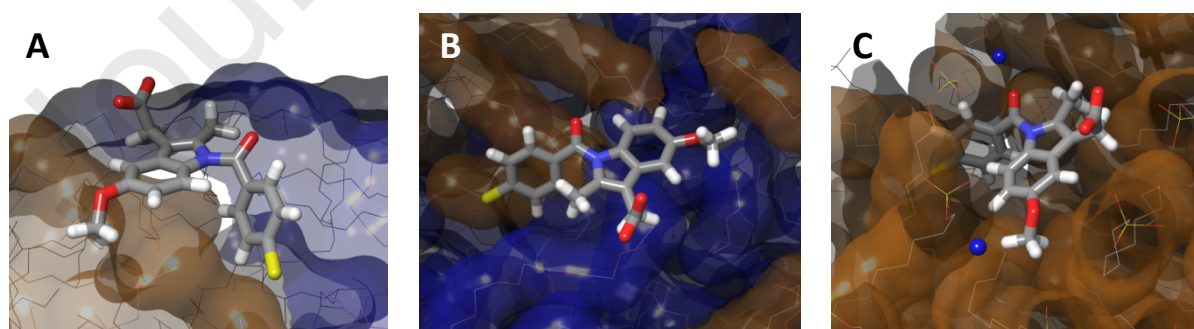
Figure 8. Snapshots at 50 ns of the MD simulation with the micelles loaded with IMC, corresponding to Pluronic® F-127 (a), Tween 20 (b) and SLS (c). IMC is represented in thick tubes, and explicit water molecules have been removed for clarity. PEO polar chains are represented as blue surfaces and hydrophobic PPO, lauryl chains are shown as orange surfaces. Sodium ions are shown as blue spheres in the SLS system.

13

Probing drug solubilization within the micelles via NMR spectroscopy.

Below we discuss properties of the drug and surfactants that affect the solubilization of the drug within the micelles in the context of NMR data and complementary results from other analytical techniques (see summarizing Figure 9).
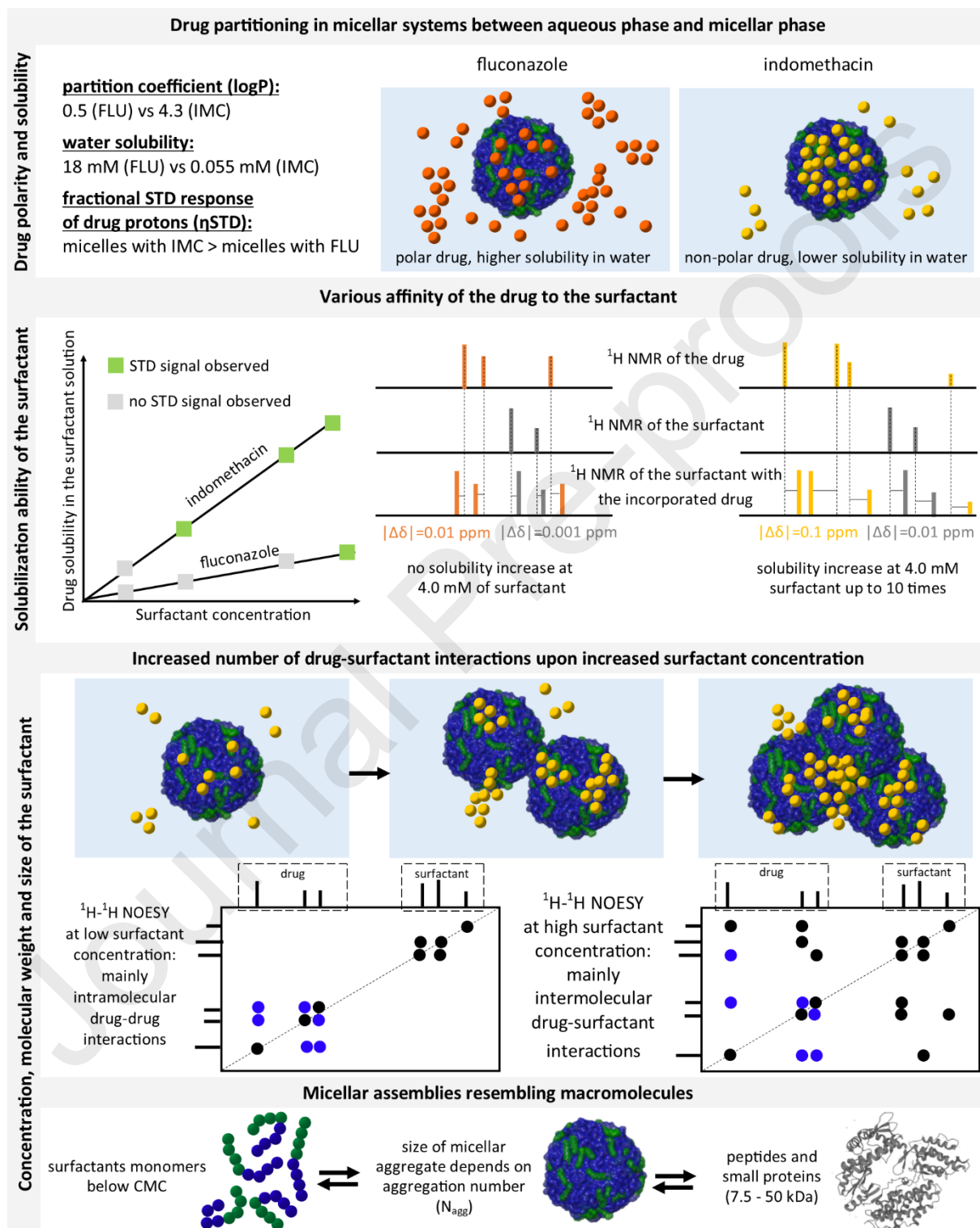
Figure 9. Properties of the drug and surfactants enabling effective drug solubilization within the micelles

Compared to IMC, FLU displayed a weaker affinity to the surfactant molecules as demonstrated in 1D and 2D NMR as well as STD measurements regardless of the surfactant used or its concentration. As FLU is more soluble in water in comparison to IMC (logP = 0.5[49] *vs*. 4.3[50]; water solubility 18.0 mM *vs*. 0.055 mM as established by HPLC, Figure 5) one may expect FLU undergoes fast exchange between aqueous and micellar phases while IMC with higher logP interacts preferably with micelles.

Even the addition of small quantities of surfactant to IMC solution resulted in substantial increase in IMC solubility (Figure 4). For example, IMC solubility in Pluronic® F-127 at 4.0 mM increased 10 times compared to its water solubility (0.55 mM vs. 0.055 mM) while in both Tween 80 and Tween 20 the drug's solubility increased 6.7 and 4.4 times respectively (0.37 mM and 0.24 mM IMC at 4.0 mM of each Tween). Although the smallest solubility increase of IMC (*i.e.* 1.7 times (0.091 mM)) was observed at 4.0 mM SLS (i.e. below its CMC value, ESI, Figure S40), increasing the surfactant concentration above CMC (173 mM which means *ca*. 20-25xCMC) resulted in *ca.* 91 times higher IMC solubility (5.0 mM and 0.055 mM respectively). On the contrary at 4.0 mM surfactant concentration maximum FLU solubility was determined as 20.8 mM (Tween 80), 18.7 mM (Pluronic® F-127), 18.6 mM (Tween 20) and 18.5 mM (SLS) as compared to 18.0 mM FLU water solubility indicating only minor FLU solubility increase (from 1.03 to 1.16 times) (ESI, Figure S28). These results were consistent with the findings reported by Nguyen-Kim *et al*.[51] The solubility of model carbamazepine (logP = 2.1-2.7) and fenofibrate (logP = 5.2) in Pluronic micelles was significantly higher for poorly water soluble fenofibrate than for carbamazepine.[51] Varshoaz *et al*.[52] reported that doxorubicin (logP = 0.9-1.4) solubilized within Pluronic micelles exhibited low partition coefficient between water and micelles. The drug solubility results agree with previously reported observations that the longer the hydrophobic chain of the surfactants, the larger the solubilization increases for both polar and non-polar drugs.[48]

Drug partitioning into micellar phase can be correlated with the changes in chemical shift values of each component.

IMC incorporated micelles in comparison to FLU loaded micelles displayed more significant changes in ^{1}H NMR chemical shifts of drug protons ($\Delta\delta$ 10^{-1} *vs*. 10^{-2}) (Figure 9). In case of IMC that interacts with micelles more strongly, the 10 times larger changes in the chemical shift perturbations for selected protons were observed as compared to FLU regardless of surfactant used. In 4.0 mM Pluronic® F-127 loaded with 19 mM FLU i.e. the maximum drug solubility in that formulation (Figure 5), 0.015 ppm change in chemical shift of multiplet H_{c+e} was observed while 0.54 mM IMC addition (its maximum solubility within 4.0 mM Pluronic® F-127 solution) resulted in 0.22 ppm shift of H_e proton of indole ring (Figure 3-4 and ESI, Figure S38). Similar observations were made for both Tween systems (Figure 3-4 and ESI, Figure S29 and S38).

Similar differences in the magnitude of ^{1}H chemical shifts perturbations were observed for surfactant peaks in the drug loaded formulations. Methyl protons in propoxy group of 2.4 mM Pluronic® F-127 were shifted by a maximum of 0.013 ppm in case of IMC series in comparison to a maximum shift of 0.006 ppm in FLU series. In Tween 20 and Tween 80 micellar systems addition of FLU and IMC caused maximum 0.02 ppm and 0.05 ppm change of surfactant protons at 41 mM and 38 mM, respectively (signal 4 of Tweens in Figure 1a). Such differences were less apparent in SLS micellar systems (ESI, Figure S29 and S37).

The cross-relaxation signals indicate formation of drug-surfactant assemblies.

Correlating solubility data with cross-relaxation peaks in NOESY spectra enabled us to observe that the enhancement of the drug solubility resulted in the presence of same phase as diagonal intermolecular drug-surfactant cross-peaks. As a consequence of higher polarity and better water solubility, the majority of FLU molecules was in the free state rather than interacting with micelles. These data were in line with the previous findings[53] that solubilizate is present in micelles and in the solution rather than being exclusively dissolved in the solution below its solubility concentration and only after exceeding that value begins to be solubilized within micelles. Hence, in FLU micellar solutions intramolecular FLU cross-peaks in 2D NOESY had the opposite sign to the diagonal indicating fast tumbling rate. This can also explain that little saturation transfer was observed in FLU incorporated micelles (η_{STD} <1%). In contrast, the preferable localization of IMC within the micelles can be concluded from 2D NOESY spectra where intramolecular drug-drug cross-peaks had the same phase as the

diagonal, indicating the drug experienced the tumbling rate similar to macromolecular aggregates. The size of the micelles and the aggregation number strongly depend on both the surfactant and its concentration as observed in TEM images and DLS measurements (e.g. at 1.6 mM Pluronic® F-127 up to 89 molecules are expected to form a micelle, while for Tween 20 and Tween 80 22 and 27 molecules form micelles below 0.9 M and 60-90 SLS molecules assemble in the 20-173 mM range).[54–56] Taking into account the molecular weight and the aggregation number of the investigated surfactants,[54–56] all analyzed assemblies resembled macromolecules. Approximated masses of the micellar aggregates ranged from around 2 to 150 times of peptide mass (*ca*. 7.5 kDa). Macromolecules show a low tumbling rate and short transverse relaxation times. Upon binding to micellar aggregates the drug acquires its tumbling rate, leading to the lowering its own T_2. This phenomenon was observed in ^{1}H NMR spectra as broadening of drug NMR signals (e.g. Figure 4c, 4f, and ESI, Figure S24c, g). In samples at concentration near the CMC values where the drug was soluble to a small extent, only drug-drug and surfactant-surfactant intramolecular cross-peaks were present.

The map of preferential drug–micelle interactions can be obtained via DEEP-STD NMR.

The irradiation of the hydrophilic or hydrophobic parts of the micelles structure enabled us to obtain the map of drug micelles interactions within minutes. This is particularly important at low ratios of drug to surfactant concentrations (resulting in low signal to noise) or spectral crowding that makes application of standard 2D NOESY techniques challenging. As this method was applied here for the first time, several practical aspects needed to be addressed. Firstly, the surfactant concentration required to obtain distinct STD NMR signals was much higher compared to the protein concentration when probing protein-ligand interactions (where 10-50 μM of protein was normally used).[57] Furthermore, to probe protein-ligand interactions by STD NMR, a [protein]:[ligand] ratio of 1:50 to 1:20 was generally used,[57] while the molar ratio between surfactant and the drug in the investigated formulations (where STD signal detected) was larger than 1 (see ESI, Table S12-S13, S15-S17). This, however, did not indicate an excess of the receptor with respect to the ligand, as a receptor was a supramolecular assembly formed in the solution *in situ* by a large number of aggregated molecules. Based on the available reports one can assume that 27 Tween 80 molecules can form a stable micelle, therefore corrected [micelle]:[drug] ratio (7.6 mM Tween 80 to 13.1 mM FLU, Table S13) was not 1:1.7, but 1:46 once the aggregation number was taken into account. Therefore the true [surfactant]:[drug] (followed by [micelle]:[drug]) ratio in micellar formulations was close to the value used to probe protein-drug interactions (i.e. 1:50).

The size of the surfactant moieties and their packing density play an important role in the saturation transfer to the drug. Among investigated surfactants, Pluronic® F-127 (*ca.* 12.6 kD) have the highest molecular weight that resembles a small protein in size. Therefore, STD signals were already observed in FLU formulations with Pluronic® F-127 at *ca.* 4.0 mM surfactant concentration, whereas higher concentration were needed in case of the Tweens, namely 7.6 mM for Tween 80 and 24 mM for Tween 20 (ESI, Table S11-S13 and Figure S41-S43). In case of dynamic assemblies formed by low molecular weight SLS (288 g/mol) the saturation transfer to hydrophilic FLU was not detected across investigated formulations.

STD signals in IMC series were observed only after saturation of SLS methylene protons at 1.2 ppm (signal 2 at Figure 1a, ESI, Table S18). This agrees well with the preferable localization of IMC within the micelle core. These proton sites experienced the largest Δδ and cross-peaks in ^{1}H-^{1}H NOESY spectra indicated their proximity to drug protons (ESI, Figure S29d and Figure S36b). The lack of the saturation transfer from the hydrophilic part of SLS can be explained by repulsion between the negatively charged sulphate groups and IMC carboxylate, in agreement with MD simulations. Furthermore, STD signals were detected for IMC series in some cases even below the CMC values of neat surfactants (ESI, Table S15-S17 and Figure S44-S46) while in FLU containing materials much higher drug concentrations had to be reached for STD signal to be detectable. As indicated by Sharp *et al*.,[53] the presence of molecules with hydrophobic properties stimulated formation of micelles resulting in lowering CMC that is known as hydrophobic effect.[45] We also observed such effect during surface tension measurements of FLU surfactant solutions during micellization (ESI, Section 6). It could have even greater effect in series loaded with hydrophobic IMC as its solubility increased substantially even at low surfactant concentrations. The effect of temperature on application of DEEP-STD NMR is discussed in ESI (ESI, Section 7).

CONCLUSIONS

In this work, structure, assembly and interactions underlying partitioning of small molecule guests within micelles were investigated by NMR spectroscopy supported by complementary analytical techniques and MD simulations. Eight model micellar systems composed of structurally distinct surfactants (ionic, nonionic, block polymer) with different aggregation properties (CMC values, aggregation numbers) and two small molecule drugs (FLU and IMC) differing in their partition coefficient were used as models to understand the molecular processes that drive drug partitioning within micellar systems.

The NMR data supported by atomistic MD simulations of micelles interacting with the small molecule drugs indicate that the frequently adopted core-shell model does not hold true for polymeric micelles composed of polyoxyethylene derivatives, used often in pharmaceutical drug delivery. In the case of Pluronic® F 127 and Tween 20 block surfactants compact micellar assemblies were formed. The repulsion between hydrophilic and hydrophobic moieties in those surfactants does not induce a layered segregation of micelles, offering a surface composed of both hydrophilic and hydrophobic domains. These differed from the structure formed by low molecular weight surfactant such as SLS. Correlation of 2D NOESY and multifrequency DEEP-STD NMR at different drug-surfactant ratios with solubility data provided mechanistic insights into formation of drug-micelles aggregates enabling us to elucidate whether the drug was preferably located in an aqueous or micellar phase. Efficient drug micellar solubilization was observed for IMC that has a higher logP than FLU. For both drugs, the solubilization ability of surfactants was in the following order SLS > Tween 80 > Tween 20 > Pluronic® F-127.

We propose that this methodology can be a valuable tool in fast screening of drug-micelle interactions. Mapping drug-surfactant interactions using 1D, 2D and multifrequency DEEP-STD NMR combined with complementary analytical techniques provides a molecular level understanding of the transient host-guest interactions in soft materials. The proposed methodology can be translated to other soft nanomaterials (e.g. nanovesicles and liposomes) to accelerate the knowledge-based design of advanced nanosized drug delivery systems and partitioning processes taking place in biological systems.

ACKNOWLEDGMENT

REFERENCES

1. Cao, J., Huang, D. & Peppas, N. A. Advanced engineered nanoparticulate platforms to address key biological barriers for delivering chemotherapeutic agents to target sites. *Adv. Drug Deliv. Rev.* **167**, 170–188 (2020).

2. Ghezzi, M. *et al. Polymeric micelles in drug delivery: An insight of the techniques for their characterization and assessment in biorelevant conditions*. *Journal of Controlled Release* **332**, 312–336 (2021).

3. Guo, R., Li, K., Qin, J., Niu, S. & Hong, W. Development of polycationic micelles as an efficient delivery system of antibiotics for overcoming the biological barriers to reverse multidrug resistance in: Escherichia coli. *Nanoscale* **12**, 11251–11266 (2020).

4. De Oliveira, C. *et al.* Micellar solubilization of drugs. *J Pharm Pharm. Sci* **8**, 147–163 (2005).

5. Li, X., Uppala, V. V. S., Cooksey, T. J., Robertson, M. L. & Madsen, L. A. Quantifying Drug Cargo Partitioning in Block Copolymer Micelle Solutions. *ACS Appl. Polym. Mater.* **2**, 3749–3755 (2020).

17

6. Becker, W., Bhattiprolu, K. C., Gubensäk, N. & Zangger, K. Investigating Protein–Ligand Interactions by Solution Nuclear Magnetic Resonance Spectroscopy. *ChemPhysChem* **19**, 895–906 (2018).

7. Gossert, A. D. & Jahnke, W. NMR in drug discovery: A practical guide to identification and validation of ligands interacting with biological macromolecules. *Prog. Nucl. Magn. Reson. Spectrosc.* **97**, 82–125 (2016).

8. Purslow, J. A., Khatiwada, B., Bayro, M. J. & Venditti, V. NMR Methods for Structural Characterization of Protein-Protein Complexes. *Front. Mol. Biosci.* **7**, 1–8 (2020).

9. Ramalhete, S. M. *et al.* Supramolecular Amino Acid Based Hydrogels: Probing the Contribution of Additive Molecules using NMR Spectroscopy. *Chem. - A Eur. J.* **23**, 8014–8024 (2017).

10. Escuder, B., LLusar, M. & Miravet, J. F. Insight on the NMR study of supramolecular gels and its application to monitor molecular recognition on self-assembled fibers. *J. Org. Chem.* **71**, 7747–7752 (2006).

11. Hu, J., Xu, T. & Cheng, Y. NMR insights into dendrimer-based host-guest systems. *Chem. Rev.* **112**, 3856–3891 (2012).

12. Sayed, M. & Pal, H. An overview from simple host–guest systems to progressively complex supramolecular assemblies. *Phys. Chem. Chem. Phys.* **23**, 26085–26107 (2021).

13. Williamson, M. P. Chemical shift perturbation. in *Modern Magnetic Resonance* 995–1012 (2018). doi:10.1007/978-3-319-28388-3_76

14. Ma, J., Guo, C., Tang, Y. & Liu, H. 1 H NMR Spectroscopic Investigations on the Micellization and Gelation of PEO–PPO–PEO Block Copolymers in Aqueous Solutions. *Langmuir* **23**, 9596–9605 (2007).

15. Saveyn, P. *et al.* Solubilization of flurbiprofen within non-ionic Tween 20 surfactant micelles: a 19F and 1H NMR study. *Phys. Chem. Chem. Phys.* **11**, 5462–5468 (2009).

16. Verbrugghe, M. *et al.* Solubilization of flurbiprofen with non-ionic Tween20 surfactant micelles: A diffusion 1H NMR study. *Colloids Surfaces A Physicochem. Eng. Asp.* **372**, 28–34 (2010).

17. Ma, J. *et al.* Micellization in aqueous solution of an ethylene oxide-propylene oxide triblock copolymer, investigated with 1H NMR spectroscopy, pulsed-field gradient NMR, and NMR relaxation. *J. Colloid Interface Sci.* **312**, 390–396 (2007).

18. Ghosh, A., Bera, S., Shai, Y., Mangoni, M. L. & Bhunia, A. NMR structure and binding of esculentin-1a (1–21)NH2 and its diastereomer to lipopolysaccharide: Correlation with biological functions. *Biochim. Biophys. Acta - Biomembr.* **1858**, 800–812 (2016).

19. Sinha, S., Zheng, L., Mu, Y., Ng, W. J. & Bhattacharjya, S. Structure and Interactions of A Host Defense Antimicrobial Peptide Thanatin in Lipopolysaccharide Micelles Reveal Mechanism of Bacterial Cell Agglutination. *Sci. Rep.* **7**, 17795 (2017).

20. Saravanan, R. *et al.* NMR Structure of Temporin-1 Ta in Lipopolysaccharide Micelles: Mechanistic Insight into Inactivation by Outer Membrane. *PLoS One* **8**, e72718 (2013).

21. Saravanan, R. *et al.* Structure, activity and interactions of the cysteine deleted analog of tachyplesin-1 with lipopolysaccharide micelle: Mechanistic insights into outer-membrane permeabilization and endotoxin neutralization. *Biochim. Biophys. Acta - Biomembr.* **1818**, 1613–1624 (2012).

22. Bhunia, A. & Bhattacharjya, S. Mapping residue-specific contacts of polymyxin B with lipopolysaccharide by saturation transfer difference NMR: Insights into outer-membrane disruption and endotoxin neutralization. *Biopolymers* **96**, 273–287 (2011).

23. Bhunia, A., Domadia, P. N. & Bhattacharjya, S. Structural and thermodynamic analyses of the interaction between melittin and lipopolysaccharide. *Biochim. Biophys. Acta - Biomembr.* **1768**, 3282–3291 (2007).

18

24. Bhunia, A., Bhattacharjya, S. & Chatterjee, S. Applications of saturation transfer difference NMR in biological systems. *Drug Discov. Today* **17**, 505–513 (2012).

25. Mayer, M. & Meyer, B. Characterization of ligand binding by saturation transfer difference NMR spectroscopy. *Angew. Chemie - Int. Ed.* **38**, 1784–1788 (1999).

26. Mayer, M. & Meyer, B. Group epitope mapping by saturation transfer difference NMR to identify segments of a ligand in direct contact with a protein receptor. *J. Am. Chem. Soc.* **123**, 6108–6117 (2001).

27. Monaco, S., Tailford, L. E., Juge, N. & Angulo, J. DiffErential EPitope mapping by STD NMR spectroscopy (DEEP-STD NMR) to reveal the nature of protein-ligand contacts. *Angew. Chemie Int. Ed.* **56**, 15289–15293 (2017).

28. Amani, A., York, P., De Waard, H. & Anwar, J. Molecular dynamics simulation of a polysorbate 80 micelle in water. *Soft Matter* **7**, 2900–2908 (2011).

29. Liu, Y. *et al.* Enhanced solubility of bisdemethoxycurcumin by interaction with Tween surfactants: Spectroscopic and coarse-grained molecular dynamics simulation studies. *J. Mol. Liq.* **323**, 115073 (2021).

30. Kopanichuk, I. V., Vedenchuk, E. A., Koneva, A. S. & Vanin, A. A. Structural properties of span 80/tween 80 reverse micelles by molecular dynamics simulations. *J. Phys. Chem. B* **122**, 8047–8055 (2018).

31. Pérez-Sánchez, G. *et al.* Rationalizing the Phase Behavior of Triblock Copolymers through Experiments and Molecular Simulations. *J. Phys. Chem. C* **123**, 21224–21236 (2019).

32. Shih, K. C. *et al.* What causes the anomalous aggregation in pluronic aqueous solutions? *Soft Matter* **14**, 7653–7663 (2018).

33. Joshi, S. Y. & Deshmukh, S. A. A review of advancements in coarse-grained molecular dynamics simulations. *Mol. Simul.* **47**, 786–803 (2021).

34. Marrink, S. J., De Vries, A. H. & Mark, A. E. Coarse Grained Model for Semiquantitative Lipid Simulations. *J. Phys. Chem. B* **108**, 750–760 (2004).

35. Muller, M. P. *et al.* Characterization of Lipid–Protein Interactions and Lipid-Mediated Modulation of Membrane Protein Function through Molecular Simulation. *Chem. Rev.* **119**, 6086–6161 (2019).

36. *Handbook of Pharmaceutical Excipients*. *Pharmaceutical Press and American Pharmacists Association* (2006).

37. Akash, M. S. H. & Rehman, K. Recent progress in biomedical applications of Pluronic (PF127): Pharmaceutical perspectives. *J. Control. Release* **209**, 120–138 (2015).

38. Cagel, M. *et al.* Polymeric mixed micelles as nanomedicines: Achievements and perspectives. *Eur. J. Pharm. Biopharm.* **113**, 211–228 (2017).

39. Amjad, M. W., Kesharwani, P., Mohd Amin, M. C. I. & Iyer, A. K. Recent advances in the design, development, and targeting mechanisms of polymeric micelles for delivery of siRNA in cancer therapy. *Prog. Polym. Sci.* **64**, 154–181 (2017).

40. Raval, A., Pillai, S. A., Bahadur, A. & Bahadur, P. Systematic characterization of Pluronic® micelles and their application for solubilization and in vitro release of some hydrophobic anticancer drugs. *J. Mol. Liq.* **230**, 473–481 (2017).

41. Patel, K. *et al.* Salt induced micellization of very hydrophilic PEO–PPO–PEO block copolymers in aqueous solutions. *Eur. Polym. J.* **43**, 1699–1708 (2007).

42. Crison, J. R., Weiner, N. D. & Amidon, G. L. Dissolution media for in vitro testing of water-insoluble drugs: Effect of surfactant purity and electrolyte on in vitro dissolution of carbamazepine in aqueous solutions of sodium lauryl sulfate. *J. Pharm. Sci.* **86**, 384–388 (1997).

43. Zhang, Q. *et al.* NMR Method for Accurate Quantification of Polysorbate 80 Copolymer Composition. *Anal. Chem.* **87**, 9810–9816 (2015).

44. Vinarov, Z., Katev, V., Radeva, D., Tcholakova, S. & Denkov, N. D. Micellar solubilization of poorly water-soluble drugs: effect of surfactant and solubilizate molecular structure. *Drug Dev. Ind. Pharm.* **44**, 677–686 (2018).

45. Holmberg, K., Jönsson, B., Kronberg, B. & Lindman, B. *Surfactants and Polymers in Aqueous Solution*. *John Wiley & Sons Ltd* (2004). doi:10.1002/0470856424.ch2

46. Angulo, J. & Nieto, P. M. STD-NMR: application to transient interactions between biomolecules—a quantitative approach. *Eur. Biophys. J.* **40**, 1357–1369 (2011).

47. Angulo, J., Enríquez-Navas, P. M. & Nieto, P. M. Ligand-Receptor Binding Affinities from Saturation Transfer Difference (STD) NMR Spectroscopy: The Binding Isotherm of STD Initial Growth Rates. *Chem. - A Eur. J.* **16**, 7803–7812 (2010).

48. Vinarov, Z., Katev, V., Radeva, D., Tcholakova, S. & Denkov, N. D. Micellar solubilization of poorly water-soluble drugs: effect of surfactant and solubilizate molecular structure Micellar solubilization of poorly water-soluble drugs: effect of surfactant and solubilizate molecula. *Drug Dev. Ind. Pharm.* **44**, 677–686 (2017).

49. Jezequel, S. G. Fluconazole: Interspecies Scaling and Allometric Relationships of Pharmacokinetic Properties. *J. Pharm. Pharmacol.* **46**, 196–199 (1994).

50. Pyka, A., Babuśka, M. & Zachariasz, M. A comparison of theoretical methods of calculation of partition coefficients for selected drugs. *Acta Pol. Pharm. - Drug Res.* **63**, 159–167 (2006).

51. Nguyen-Kim, V. *et al.* Solubilization of active ingredients of different polarity in Pluronic® micellar solutions - Correlations between solubilizate polarity and solubilization site. *J. Colloid Interface Sci.* **477**, 94–102 (2016).

52. Varshosaz, J., Hassanzadeh, F., Sadeghi-aliabadi, H., Larian, Z. & Rostami, M. Synthesis of Pluronic® F127-poly (methyl vinyl ether-alt-maleic acid) copolymer and production of its micelles for doxorubicin delivery in breast cancer. *Chem. Eng. J.* **240**, 133–146 (2014).

53. Sharp, M. A., Washington, C. & Cosgrove, T. Solubilisation of model adjuvants by Pluronic block copolymers. *J. Colloid Interface Sci.* **344**, 438–446 (2010).

54. Sharma, P. K. & Bhatia, S. R. Effect of anti-inflammatories on Pluronic® F127: Micellar assembly, gelation and partitioning. *Int. J. Pharm.* **278**, 361–377 (2004).

55. Acharya, K. R., Bhattacharya, S. C. & Moulik, S. P. The surfactant concentration-dependent behaviour of safranine T in Tween (20, 40, 60, 80) and Triton X-100 micellar media. *J. Photochem. Photobiol. A Chem.* **109**, 29–34 (1997).

56. Hammouda, B. Temperature Effect on the Nanostructure of SDS Micelles in Water. *J. Res. Natl. Inst. Stand. Technol.* **118**, 151–167 (2013).

57. Walpole, S., Monaco, S., Nepravishta, R. & Angulo, J. STD NMR as a Technique for Ligand Screening and Structural Studies. *Methods Enzymol.* **615**, 423–451 (2019).

Declaration of interests

☐ The authors declare that they have no known competing financial interests or personal relationships that could have appeared to influence the work reported in this paper.

☒ The authors declare the following financial interests/personal relationships which may be considered as potential competing interests: